JOURNAL OF MATERIALS SCIENCE 28 (1993) 860–864

Carbon dioxide decomposition into carbon with the rhodium-bearing magnetite activated by H_2-reduction

K. AKANUMA, K. NISHIZAWA, T. KODAMA, M. TABATA, K. MIMORI, T. YOSHIDA, M. TSUJI, Y. TAMAURA
Department of Chemistry, Research Center for Carbon Recycling and Utilization, Tokyo Institute of Technology, Ookayama, Meguro-ku, Tokyo 152, Japan

The CO_2 decomposition into carbon with the rhodium-bearing activated magnetite (Rh-AM) was studied in comparison with the activated magnetite (AM). The Rh-AM and the AM were prepared by flowing hydrogen gas through the rhodium-bearing magnetite (Rh-M) and the magnetite (M), respectively. The rate of activation of the Rh-M to the Rh-AM was about three times higher than that of the M to the AM at 300 °C. The reactivity for the CO_2 decomposition into carbon with the Rh-AM (70% CO_2 was decomposed in 40 min) was higher than that with the AM (30% in 40 min) at 300 °C. The Rh-M was activated to the Rh-AM at a lower temperature of 250 °C, and the Rh-AM decomposed CO_2 into carbon at 250 °C. On the other hand, the M was little activated at 250 °C.

1. Introduction

The reduction of CO_2 has been extensively studied by many investigators using chemical, physical and biological methods. However, reports of the decomposition of CO_2 into carbon are very few [1–4]. Sacco and Reid [1] reported the deposition of carbon on the surface of iron catalyst during the decomposition of CO_2 gas with hydrogen gas using metal iron as the catalyst at 527–627 °C (Bosch reaction). In this reaction, metal iron decomposed CO_2 into carbon in the presence of hydrogen gas at the high temperatures, and the iron oxides (magnetite and wüstite) were formed in the iron catalyst. In the Bosch reaction studied by Wagner *et al.* [2], CO_2 and hydrogen were reacted with iron metal at 426–726 °C, and by-products such as CO and CH_4 were formed with a CO_2 decomposition efficiency around 10%–20%. Lee *et al.* [3] reported that the metal iron was transformed into a mixture of iron oxide (magnetite) and carbides progressively in the decomposition reaction of CO_2 gas into carbon with hydrogen gas using metal iron. Copperthwaite *et al.* [4] studied the decomposition reaction of CO_2 on the surface of the metals using X-ray photoelectron spectroscopy. Thus, the CO_2 decomposition reaction reported so far is accompanied by the side reactions, such as the hydrogenation of CO_2 and the formation of the carbides, and there have been no reports on the complete decomposition of CO_2 with efficiency approaching 100%.

When we preliminarily studied the CO_2 decomposition with metals, we found that no CO_2 was decomposed below 250 °C with metals such as magnesium, aluminium and copper, and that only a small amount of CO_2 was decomposed at 290 °C (3% after 6 h reaction) [5]. Recently, we have reported that the activated magnetite, which had been obtained by flowing hydrogen gas through the magnetite at 290 °C, can decompose CO_2 gas into carbon with a high efficiency (nearly 100%) at 290 °C [6]. In this reaction, we estimated that the oxygen of the CO_2 gas is transferred into the oxygen-deficient site of the activated magnetite during the deposition of carbon on the surface of the activated magnetite, and have confirmed the fact that its spinel-type structure is retained [6].

In the present work, we have studied the decomposition of CO_2 into carbon with the rhodium-bearing activated magnetite (Rh-AM), and its reactivity for the decomposition of CO_2 in comparison with the activated magnetite (AM).

2. Experimental procedure

Magnetite powder (M) was prepared by the air oxidation method; the Fe(II) hydroxide suspension (Fe (II) $= 4.8 \times 10^{-2}$ mol; $FeSO_4 \cdot 7H_2O$) was oxidized in a 3 dm^3 beaker by passing air through the reaction suspension at pH 10 and at 65 °C [7–10]. The black precipitate of the synthesized magnetite particles was washed with distilled water, and acetone successively, and dried *in vacuo* at 50 °C. The BET adsorption surface area of the powder magnetite was estimated to be 21 $m^2 g^{-1}$.

The pH titration curve for the suspension containing magnetite powder and Rh(III) ion ($RhCl_3 \cdot 3H_2O$; 0.15 mol dm^{-3}) was obtained by adding a constant volume (1.0×10^{-3} dm^3) of 0.1 mol dm^{-3} NaOH solution. The magnetite powder suspension was prepared at pH 5.0.

0022–2461

In the preparation of the rhodium-bearing magnetite (Rh-M), the magnetite powder (M) (2.0 g) was suspended in an aqueous solution (6.0×10^{-3} dm^3) of $RhCl_3 \cdot 3H_2O$ (0.15 mol dm^{-3}) at pH 5.0, and the pH of the suspension (preparation pH) was adjusted to 8.5 and 12.0 with 0.1 mol dm^{-3} NaOH solution. The precipitates were collected by decantation, washed with distilled water several times, and dried in air at 120 °C for 15 h. The samples thus obtained were subjected to X-ray diffractometry with FeK_α radiation (Rigaku RAD-2A) to identify the solid phase, and to chemical analysis. The rhodium and total iron contents in the samples were determined by atomic absorption spectroscopy, and Fe^{2+}/Fe_{total} mol ratio, by colorimetry with 2,2′-bipyridyne [11]. X-ray diffractometry and chemical analysis showed that the dried samples were the rhodium-bearing magnetite (Rh-M).

The rhodium-bearing magnetite (Rh-M) (16 mg) was placed in a quartz holder (diameter 4.7 mm × 2.7 mm), and set up in the electric furnace of the thermogravimeter (Shimadzu TGA-50). The hydrogen gas was passed through the Rh-M to obtain the activated Rh-M (Rh-AM) (flow rate = 2.0×10^{-2} dm^3 min^{-1}). The rate of the activation of the Rh-M to the Rh-AM with the hydrogen gas (activation step) was studied from the TG curves, which had been obtained under passing the hydrogen gas through the Rh-M in the thermogravimeter.

$CO_2 \rightarrow$ C decomposition reaction with the Rh-AM or AM was studied using a reaction cell in a batch system. The Rh-M or M was placed in the reaction cell (diameter 8 mm × 330 mm) and set up in an electric furnace, whose temperature was controlled to 300 ± 1 °C. After the evacuation in the reaction cell, hydrogen gas was flowed through the Rh-M or M for 2 h (flow rate = 1.0×10^{-2} dm^3 min^{-1}) to obtain the activated Rh-M (Rh-AM) or the activated M (AM). After evacuating the reaction cell again, the inlet and outlet valves were closed, and CO_2 gas (5.0×10^{-3} dm^{-3}) was injected into the reaction cell. The inner pressure of the reaction cell was measured with the pressure gauge. The inner gas species were determined by gas chromatography (Shimadzu GC-8A). Chemical analysis of the carbon deposited in a polymerized form was carried out using an elemental analyser (Perkin–Elmer 2400 CHN) for the carbon powder collected after dissolving the samples in an HCl solution. On the other hand, the carbon, which was deposited in a dispersed form, was determined by subjecting the samples directly to the elemental analyser without dissolving the samples in the HCl solution.

3. Results and discussion

Fig. 1 shows the pH titration curve of the suspension containing magnetite powder and Rh(III) ion. Samples 2 and 3 were prepared from the precipitates obtained at the points indicated by arrows for Curve A in Fig. 1. As can be seen from Curve A, the suspension was titrated in the pH range 7.5–8.5. Precipitates of hydroxide and/or oxide of Rh(III) were formed at pH 8.5 (at the point indicated by Sample 2). Samples 2 and 3 were prepared by collecting the precipitates by decantation, and washing with distilled water. In this decantation step, most of the precipitates of the hydroxide and/or oxide of Rh(III) ions were discarded.

The chemical compositions of the magnetite powder (M; Sample 1) and the rhodium-bearing magnetites (Rh-M; Samples 2 and 3) are given in Table 1. As can be seen from Table 1, the Fe(II) ion content in the Rh-M is much lower than that of the stoichiometric magnetite (Fe_3O_4; $Fe^{2+}/Fe_{total} = 0.333$), indicating that the magnetite portion of the Rh-M was oxidized into γ-Fe_2O_3. In the X-ray diffraction patterns of the Rh-M, only the strong peaks of the spinel-type compound which correspond to those of γ-Fe_2O_3 appeared. The rhodium content in Sample 3 is slightly higher than that in Sample 2. However, their Rh(III) ion amounts are about 1/50 of the Rh(III) ions in the suspension used for the pH titration. This is due to the fact that most of the Rh(III) ions were discarded as the hydroxide and/or oxide during the decantation in the Rh-M preparation. Sample 4 in Table I was prepared by mechanochemically mixing the magnetite powder with the metallic rhodium powder at room temper-

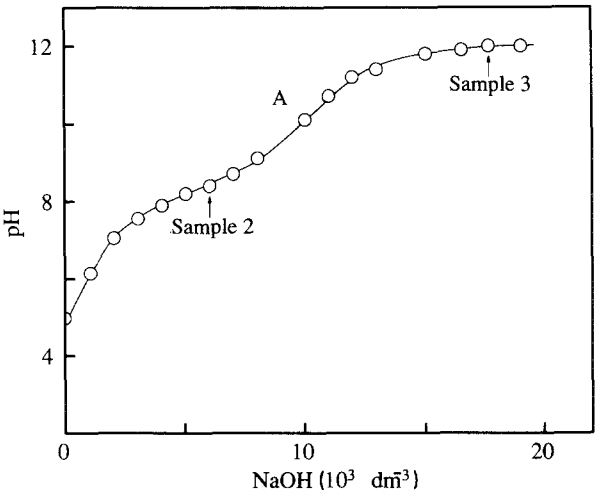

Figure 1 pH titration curve for the suspension containing magnetite powder and Rh (III) ion, which was obtained by adding a constant volume (1.0×10^{-3} dm^3) of 1.0×10^{-1} mol dm^{-3} NaOH solution.

TABLE I Chemical composition of samples

Sample	Preparation pH	Mole ratios of Rh, Fe^{2+} and Fe^{3+} to Fe_{total}		
		Rh/Fe_{total}	Fe^{2+}/Fe_{total}	Fe^{3+}/Fe_{total}
1[a]	–	–	0.26	0.74
2[b]	8.5	6.2×10^{-4}	0.02	0.98
3[b]	12.0	8.9×10^{-4}	0.08	0.92
4[c]	–	3.4×10^{-2}	0.20	0.80

[a] Magnetite powder (M).
[b] Rhodium-bearing magnetite powder (Rh-M).
[c] Magnetite powder (M) mixed mechanochemically with metallic rhodium powder.

ature. The rhodium content in Sample 4 is about 50 times higher than that in Samples 2 and 3.

Fig. 2 shows the TG curves obtained by raising the temperature from room temperature to 400 °C at 5 °C min^{-1} while passing hydrogen gas through Samples 1–4. For Sample 1 (magnetite, M; Curve A, Fig. 2), a small weight decrease was observed in the range 220–285 °C, and its weight was kept nearly constant at 285–354 °C. This weight decrease is due to the reduction of γ-Fe_2O_3 component of the M into Fe_3O_4 component (γ-$Fe_2O_3 \rightarrow Fe_3O_4$ step). Above 354 °C, the weight of Sample 1 abruptly decreased. This abrupt decrease comes from the release of the lattice oxygen of the magnetite (activation step).

As can be seen from Curves B and C (Samples 2 and 3) in Fig. 2, the γ-$Fe_2O_3 \rightarrow Fe_3O_4$ step and the activation step took place at lower temperatures than those of Sample 1 (Curve A; M). The temperatures (initiation temperature for the activation step; T_i), where the activation step begins, were estimated from the TG curves in Fig. 2, and are listed in Table II. The weight decrease in the range 100–250 °C for Curves B and C would superimpose on the reduction of Rh(III) into metallic rhodium and the γ-$Fe_2O_3 \rightarrow Fe_3O_4$ step; rhodium in the Rh-M obtained after the Rh-M preparation process is Rh(III) (Rh(III) hydroxide or $Rh_2O_3 \cdot nH_2O$). Thus, it was found that the activation of M to the AM with hydrogen reduction is enhanced by impregnation of M with rhodium (pH titration method); the Rh-M was activated at a lower temperature than that for the M.

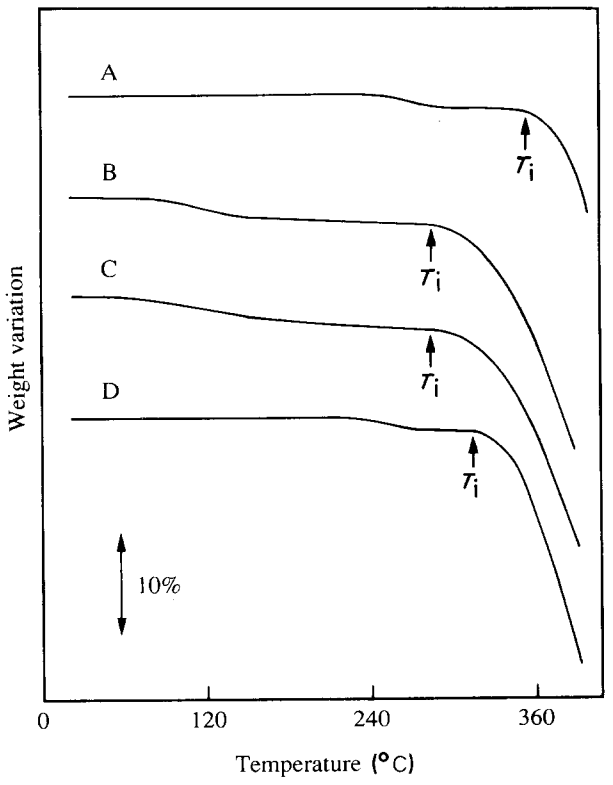

Figure 2 TG curves obtained by keeping Samples 1–4 under flowing hydrogen and by raising the temperature from room temperature to 400 °C at 5 °C min^{-1}; Curve A, Sample 1 (magnetite, M); Curves B and C, Samples 2 and 3 (Rh-M), respectively, Curve D, Sample 4 (mixture of M and metallic rhodium powder); T_i = initiation temperature for the activation step.

TABLE II Initiation temperature, T_i, for the activation evaluated from TG curves (Fig. 2), obtained by raising the temperature from room temperature to 400 °C, and the activation rate evaluated from TG curves, obtained by keeping samples at constant temperatures (250 and 300 °C) under flowing hydrogen gas

Sample	T_i(°C)	Activation rate ($-\Delta O^{2-}$ mol min^{-1})	
		300 °C	250 °C
1	354	1.7×10^{-6}	2.9×10^{-9}
2	282	5.5×10^{-6}	1.0×10^{-6}
3	281	4.2×10^{-6}	–
4	315	–	–

As can be seen from Curves B and C, similar TG curves were obtained for Samples 2 and 3, indicating that the rhodium in Samples 2 and 3 exerts an effect on the enhancement of the activation to an equal extent. This would be due to the fact that the rhodium contents in the Rh-M were nearly equal (Table I). Curve D in Fig. 2 shows the TG curve for Sample 4, which was prepared by mechanochemically mixing the magnetite powder with the metal rhodium powder. As can be seen from Table II, the T_i for Sample 4 (315 °C) is lower than that for Sample 1 (magnetite; M) (354 °C), indicating that the metallic rhodium powder, which would be attached to the magnetite powder during the mechanochemical mixing, lowers the T_i of the magnetite (M). Thus, the metallic rhodium powder enhances the activation of the M, when it is in contact with the M on the surface. This effect of the metallic rhodium on the activation of M is further enhanced by impregnation of M with the metallic rhodium as shown from T_i for Samples 2 and 3 (282, 281 °C). In the impregnation method (pH titration method), colloidal hydroxides or oxides of Rh (III) will be deposited on the surface of the M, and they are considered to be metallized in the initial stage in the TG measurement. Thus, the metallic rhodium deposited by the impregnation method has a larger surface area, which seems to exert an enhancement for activation for Samples 2 and 3. The activated magnetite, some of whose lattice oxygen are removed by the hydrogen reduction, can reduce CO_2 at 290 °C [6]. The activation is enhanced by acceleration of the removal of lattice oxygen of the M. The acceleration of the removal of the oxygen of M with the metallic rhodium will come from the dissociative adsorption of $H_2 \rightarrow 2H_{ads}$ on the surface of the metallic rhodium [12], where H_{ads} indicates adsorbed elemental hydrogen. This H_{ads} will readily react with the lattice oxygen to form H_2O, and the activation of the M will be enhanced with the metallic rhodium.

We have studied the enhancement of the activation of M and Rh-M from the TG curves, which had been obtained by keeping the samples at a constant temperature (300 °C) under hydrogen gas. The TG curves, which decreased almost linearly with hydrogen flow time (H_2 flow rate $= 2.0 \times 10^{-2}$ dm^3 min^{-1}) owing to the activation, were obtained for Samples 1 (M), and 2 and 3 (Rh-M) at 300 °C. The activation rates

evaluated from the tangent of the TG curves are given in Table II. As can be seen from Table II, the rates of activation from Rh-M to Rh-AM (Samples 2 and 3) were about three times faster than that from M to AM (Sample 1) at 300 °C.

Curves A and B in Fig. 3 show the TG curves obtained by keeping Samples 1 (Curve A; M) and 2 (B; Rh-M) under hydrogen gas at 250 °C. A rapid weight decrease in the initial stage is due to both the transformation of the γ-Fe_2O_3 component to Fe_3O_4 and the reduction of Rh(III) ion to the metallic rhodium. As shown by Curve A, the weight decrease for Sample 1 was little observed after the rapid decrease in the initiation. Thus, the M (Sample 1) was little activated by the hydrogen reduction at 250 °C. The activation rate evaluated from the tangent of the Curve A in Fig. 3 was $2.9 \times 10^{-9} O^{2-}$ mol min^{-1} (Table II). Thus, we could not efficiently activate the M, when the temperature was lowered from 300 °C to 250 °C. On the other hand, as can be seen from Curve B in Fig. 3, the Rh-M (Sample 2) was efficiently activated even at 250 °C. The activation rate is about 350 times higher than that for the M (Table II). Thus, even at 250 °C, we could efficiently activate the M by impregnation of the M with the metallic rhodium. For Sample 2 (Rh-M), the activation rate at 250 °C is about one-fifth of that at 300 °C (Table II). The activation energy for the reaction to transform from the Rh-M (Sample 2) to Rh-AM was evaluated to be 83.1 kJ mol^{-1}.

Curves A and B in Fig. 4 show the time variations of the CO_2 content (partial pressures evaluated from the gas content analysis by gas chromatography) in the reaction cell during the $CO_2 \rightarrow C$ decomposition reaction with the AM and the Rh-AM, respectively, at 300 °C. For the AM (Curve A in Fig. 4), the CO_2 content gradually decreased with reaction time, and about 50% of the CO_2 volume in the reaction cell diminished in 90 min (30% in 40 min). On the other hand, for the Rh-AM (Curve B in Fig. 4), the CO_2 content decreased with reaction time at a higher rate than for the AM (Curve A), and about 80% of the CO_2 diminished in 90 min (70% in 40 min). Thus, the activated rhodium-bearing magnetite (Rh-AM) has a higher reactivity for CO_2 decomposition than the activated magnetite (AM). The carbon content in the

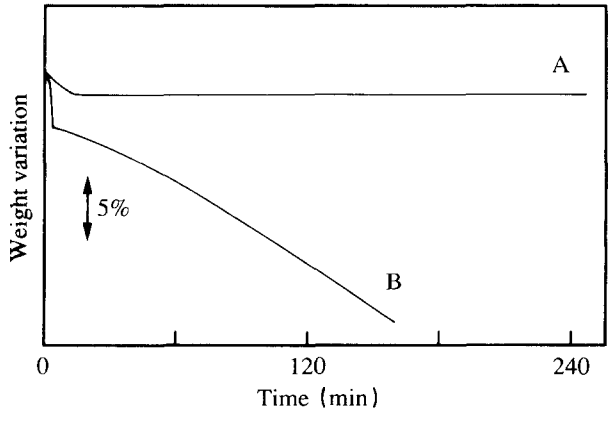

Figure 3 TG curves obtained by keeping Samples 1 (Curve A; M) and 2 (Curve B; Rh-M) under flowing hydrogen gas at constant temperature of 250 °C.

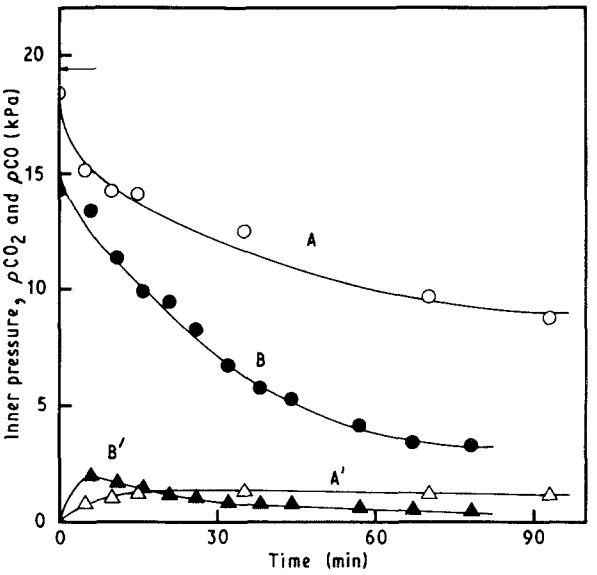

Figure 4 Time variations of the gas contents of CO_2 and CO in the reaction cell during CO_2 decomposition with AM or Rh-AM at 300 °C; Curves A (AM) and B (Rh-AM) for CO_2; Curves A′ (AM) and B′ (Rh-AM) for CO; the initial CO_2 content in the reaction cell is indicated (←).

solid samples, which had been determined by chemical analysis for the carbon powder collected after dissolving samples in the HCl solution, corresponded to 33% of the diminished CO_2 volume for AM, and 70% for Rh-AM. From the deposited carbon content determined without dissolving the samples, about 90% carbon recovery was obtained for Curves A and B. Because the diminished CO_2 volume for Curve A (AM; Fig. 4) during the CO_2 decomposition is smaller than that for Curve B (Rh-AM), the degree of the polymerization of the deposited carbon for Curve A is expected to be lower than that for Curve B, because of the lower concentration of the deposited carbon on the surface for Curve A. In the work by McCarty and Wise [13] for carbons deposited on the nickel metal catalyst, two types of carbon in the dispersed (α) and polymerized (β) forms have been reported. The α state carbon is considered to be isolated surface carbon atoms bonded to the nickel, and the β state is taken as amorphous carbon. In the present work, also we are able to consider two types of carbon deposited on the surface; one is the dispersed carbon like the α form, the other polymerized carbon like the β form. The dispersed carbon, which is not polymerized, would not be determined by the present chemical analysis after dissolving the sample in the HCl solution, because the dispersed carbon will be readily transformed into CO or CO_2 during the dissolution process. The difference in the carbon recovery between the chemical analysis with (33% for AM, 70% for Rh-AM) and without (90%) the dissolution of samples would come from a failure in the analysis of dispersed carbon in the chemical analysis.

In Fig. 4, during the decrease in the CO_2 content in the reaction cell, the inner pressure of the reaction cell also decreased in accordance with a lowering of the CO_2 content. Moreover, a small amount of CO was evolved during the reaction as given by Curves A′ and

B′ in Fig. 4. During CO_2 decomposition with the AM, the gas species in the reaction cell were only CO_2 and CO (no other gaseous products were detected by gas chromatography), and the sum of the partial pressures of CO_2 (pCO_2) and CO (pCO) was nearly equal to the inner pressure in the reaction cell. Also, during the CO_2 decomposition with the Rh-AM, the inner pressure was nearly equal to the sum of pCO_2 and pCO. These findings show that the oxygen in the CO_2 gas is transferred into the Rh-AM or the AM.

Trace amounts of CH_4 and C_2H_6 were detected by gas chromatography after 20 min CO_2 decomposition reaction with Rh-AM. This evolution of trace amounts of hydrocarbons would have occurred from CO by the reaction with hydrogen, which was generated from the traces of H_2O remaining after the activation step. H_2O is formed during the activation step for the Rh-AM, but it can be continuously removed by the hydrogen stream in the activation step. We evacuated the reaction cell after the activation step to remove H_2O, and injected CO_2 gas for the CO_2 decomposition reaction. However, it seems that it was not possible to completely remove all traces of H_2O in these processes.

The CO_2 decomposition into C with Rh-AM at 250 and 300 °C was studied using the thermogravimeter. After activation of the Rh-M by passing hydrogen gas (flow rate $= 2.0 \times 10^{-2}$ dm^3 min^{-1}) through at 250 °C (3 h) and 300 °C (40 min), CO_2 gas (flow rate $= 2.0 \times 10^{-2}$ dm^3 min^{-1}) was passed through the Rh-AM at 250 and 300 °C. The weight in the TG curve increased during flow of the CO_2 gas through the samples. This weight increase in the TG curve is due to the incorporation of oxygens in the CO_2 molecule into the Rh-AM and the deposition of carbon by the decomposition of CO_2 on the surface of Rh-AM. The weight increase rates evaluated from the TG curve for Sample 2 at 250 and 300 °C are listed in Table III. After passing CO_2 gas for 50 min, the samples were dissolved in HCl solution. We observed that the undissolved carbon powder was suspended in the HCl solution. However, the amount of carbon was too small to analyse, because the sample amount for thermogravimetry was small (15 mg). Thus, we could not quantitatively determine the amount of deposited carbon, but it was confirmed that CO_2 is decomposed into carbon. As can be seen from Table III, the CO_2 decomposition into carbon with Rh-AM takes place even at 250 °C at a fast decomposition rate of 3.8×10^{-2} wt% min^{-1}.

TABLE III Weight increase rate evaluated from TG curves, obtained by passing CO_2 gas through the Rh-AM

Temperature (°C)	Weight increase rate (% min^{-1})
250	3.8×10^{-2}
300	1.5×10^{-1}

Acknowledgement

The present work was partially supported by a Grant-in-Aid for Science Research no. 03203216 from the Ministry of Education, Science and Culture.

References

1. A. SACCO Jr and R. C. REID, *Carbon* **17** (1979) 459
2. R. C. WAGNER, R. CARRASQUILLO, J. EDWARDS and R. HOLMES, in "Proceedings of 18th Intersociety Conference on Environmental Systems", SAE Technical Paper Series 880995 (Society of Automotive Engineers, 1988).
3. M. LEE, J. LEE and C. CHANG, *J. Chem. Engng. Jpn* **23** (1990) 130
4. R. G. COPPERTHWAITE, P. R. DAVIS, M. A. MORRIS, M. W. ROBERTS and R. A. RYDER, *Catal. Lett.* **1** (1988) 11
5. Y.TAMAURA, in "Proceedings of the International Symposium on Chemical Fixation of Carbon Dioxide", Nagoya, 2–4 December 1991, p. 167
6. Y. TAMAURA and M. TABATA, *Nature* **346** (1990) 255
7. Y. TAMAURA, S. MECHAIMONCHIT and T. KATSURA, *J. Inorg. Nucl. Chem.* **43** (1980) 671
8. T. KATSURA, Y. TAMAURA and G. S. CHYO, *Bull. Chem. Soc. Jpn* **52** (1979) 96
9. Y. TAMAURA, P. V. BUDUAN and T. KATSURA, *J. Chem. Soc. Dalton Trans.* (1981) 1807
10. M. KIYAMA, *Bull. Chem. Soc. Jpn* **47** (1974) 1646
11. I. IWASAKI, T. KATSURA, T. OZAWA, M. YOSHIDA, M. MASHIMA, H. HARAMURA and B. IWASAKI, *Bull. Volcanol. Soc. Jpn. Ser. II* **5** (1960) 9
12. H. KOBAYASHI, S. YOSHIDA, H. KATO, K. FUKUI and K. TARAMA, *Surf. Sci.* **79** (1979) 189
13. J. G. McCARTY and H. WISE, *J. Catal.* **57** (1979) 406

Received 20 January
and accepted 30 June 1992